TÉCNICO LISBOA

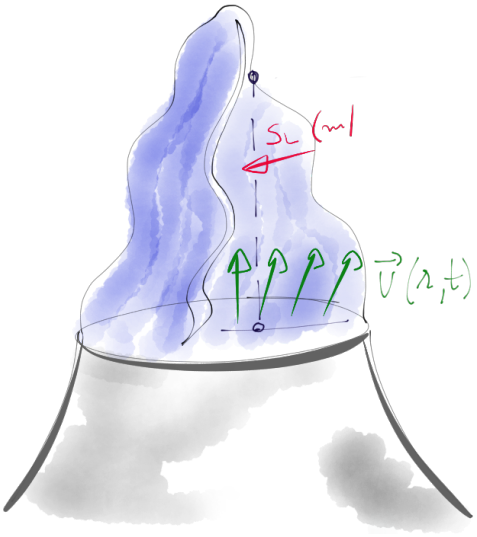


# G-Equation Modeling of Unsteady Flame Dynamics

**Edmundo Ferreira**

Thesis to obtain the Master of Science Degree in

## Aerospace Engineering

Supervisor(s): Professor Edgar Fernandes, Professora Ana Silvestre

### Examination Committee

| | |
|---|---|
| Chairperson: | Professor Full Name |
| Supervisor: | Professor Edgar Fernandes, Professora Ana Silvestre |
| Member of the Committee: | Professor Full Name 3 |

### Month and Year

# Contents

# Chapter 1

# Introduction

## 1.1 Motivation

Today, combustion processes are the power horse of the world's transport and energy production systems and in some areas such has aeronautics and fossil fuel power plants, due to their high efficiency, high thrust to weight ratios and fast response times, they are irreplaceable in the power gap from several hundred kilowatt to hundreds of megawatt. The problem is even more acute in rocket propulsion, where the demand is in the order of the gigawatt **?**.

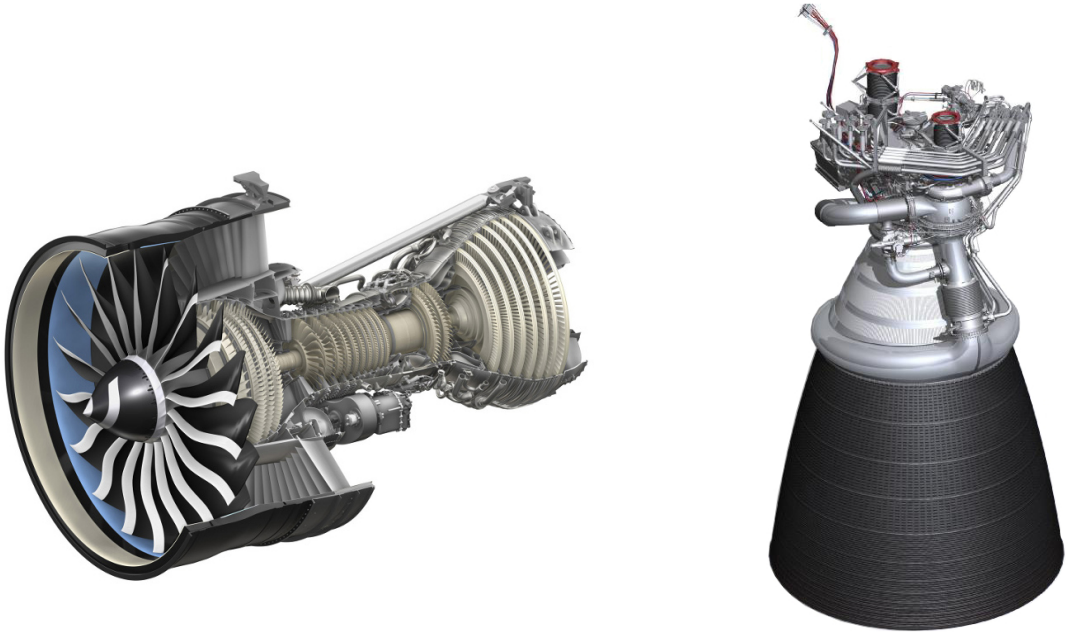

(a) GEnx turbofan engine cutaway.

(b) NASA J-2X upper stage rocket engine.

Figure 1.1: Examples of modern combustion systems on which there are no reliable technological alternatives, and where combustion instabilities are a limiting performance factor.referenciar imagens

The demand for evermore efficient, and less pollutant, specially on $NO_x$ emission, has pushed the design of some systems toward leaner and in if possible premixed combustion. Operating at lower temperatures and in conditions closer to the flammability or blowout limit, tends to aggravate the combustion

instabilities **?**, **?**, **?**, that usually results in excessive vibrations, mechanical faults, high levels of acoustic noise, high burn and heat transfer rates possibly melting the components, therefore extremely undesirable,**?**. This is the more or less the motivation behind all combustion instability studies, however the topic is complex, far from well defined and therefore very broad. We start with a brief revision of the combustion instabilities, then focus on the thermoacoustic instabilities, then link them to the G-equation formulation, a level set method for flame kinematics. During those steps we hope to make clear the areas of concern of our specific approach, as well try to frame it in wider context.

## 1.2 Combustion Instabilities Revision

Upon the bibliographic revision of combustion instabilities, several different definition arose, most of them were in fact specific to a certain type instability. The most global approaches were given by **?** and by **?**, and a conceptual summary is presented in figure 1.2.

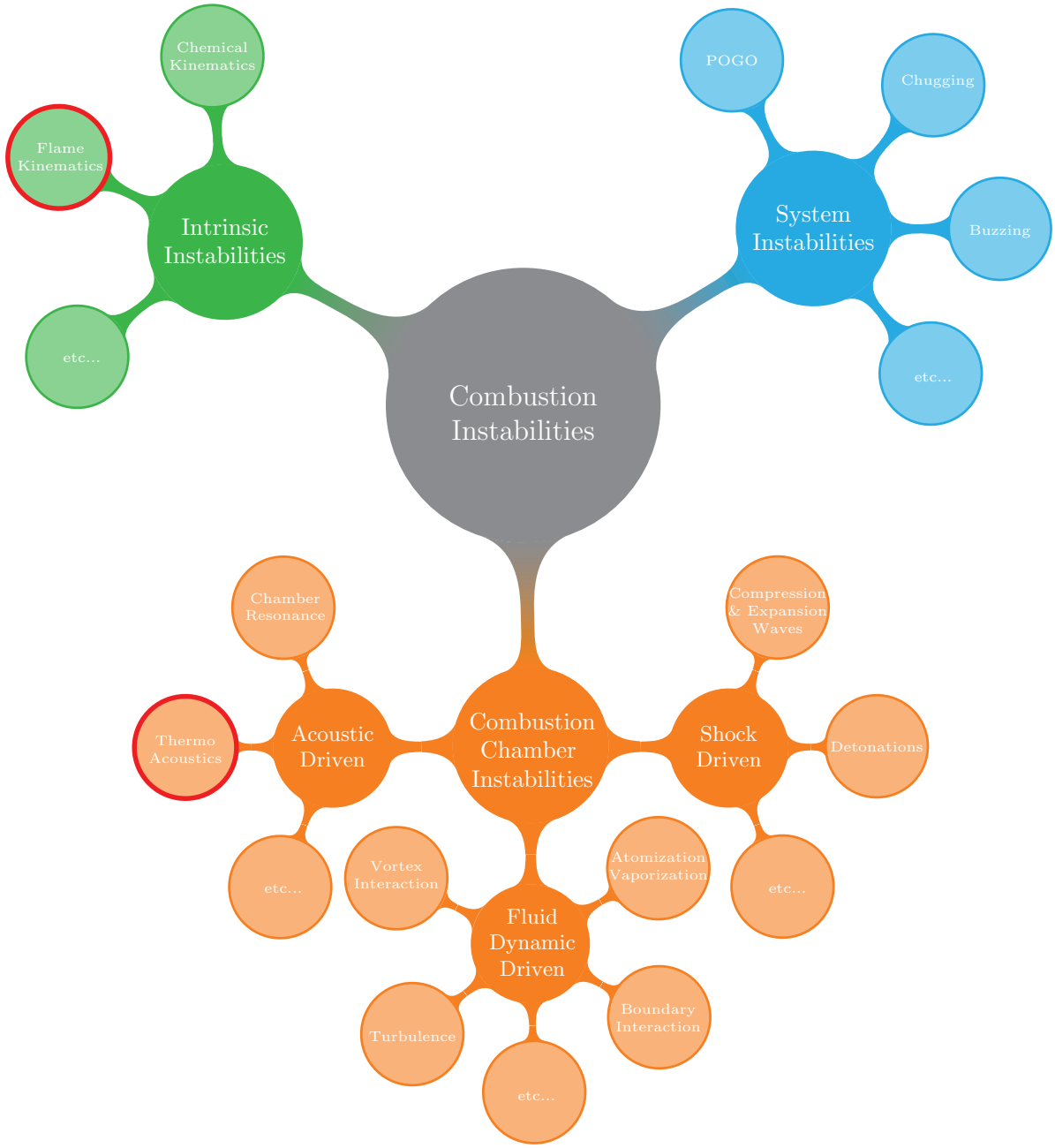


Figure 1.2: Illustrative mind-map of combustion instabilities. We present a conceptual classification according to **?**, and also examples or mechanisms of instabilities in each category. The red circles represent the topics with this study will focus on, thermoacoustics and flame kinematics instability mechanisms. change kinematics to dynamics) improve visiability

The conceptual representation of figure 1.2, was progressively created has researchers focused their attention and analysis on only a small subset of mechanisms, that dominated their specific problem.

Thus we must emphasize that the conceptual categories of figure 1.2, are in no way isolated. On the contrary, real systems should be considered has a multivariate dynamical system coupling all the above mechanism, however not all with the same intensity.

An interesting perspective shown in figure 1.2, and also described in **?** is that the instabilities can be ordered by characteristic space scales where they develop. Intrinsic instabilities are not system dependent since the usually develop in the smaller space scales, such as the local flame front, or even smaller, the chemical reaction scales. In the combustion chamber instabilities some of major effects are driven by the fluid flow, acoustic or shock wave interactions inside the chamber. In a even larger space scales we have system instabilities, that act on space scale of the heater, engine, turbine, rocket or even in the entire launch vehicle. These larger space scales of combustion instabilities drivers, can influence or be triggered by the lower ones thus creating a very complex interaction of cause's and effects.

In this report we restrict ourselves to thermoacoustic and flame kinematic coupling, and try to improve the models for application where these phenomena are the prime drivers of combustion instabilities.

## 1.3 Thermoacoustic Instabilities

In a control theory analogy thermoacoustic instabilities are acoustic waves (pressure, velocity or density) coupled with heat release fluctuations. The major source of the heat release is the flame and thus it's kinematics strongly influence dynamical response of the system, as presented in figure 1.3, inspired by **?** and specially by **?**.

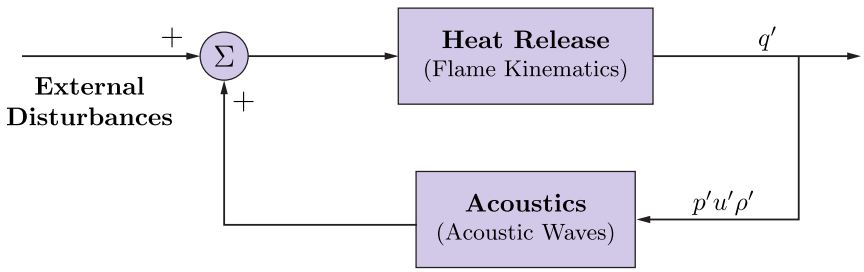


Figure 1.3: Schematic diagram of thermoacoustic combustion instabilities as a feedback amplifier between acoustic waves, and heat release emanating from the flame front.

# Chapter 2

# Theoretical and Computational Methods

## 2.1 G-Equation Formulation

### 2.1.1 General G-Equation

The G-Equation formalism is no more than a mathematical construct of the flame front as an "infinitesimal" surface, thus only yields physical representation for flames the have "thin" flame fronts. The flame as a mathematical surface, corresponds to a function $G(\mathbf{x}, t)$, that for all points of the flame front $\mathbf{x} \equiv \mathbf{x}_f$ in a given time $t$, is equal to constant $G_0$, i.e. the flame front is the level set function has defined in (2.1).

**Definition 2.1.1** (**Level Set Function).**

$$\begin{aligned} G(\mathbf{x} \equiv \mathbf{x}_f, t) = G_0 \quad & \textbf{unsteady flame front} \\ G(\mathbf{x}, t) > G_0 \quad & \textbf{product side} \\ G(\mathbf{x}, t) < G_0 \quad & \textbf{reacting side} \end{aligned} \tag{2.1}$$

$$\textit{with} \qquad G : \mathbb{R}^4 \longrightarrow \mathbb{R}, \quad G_0 \in \mathbb{R}, \quad \mathbf{x} \in \mathbb{R}^3, \quad t \in \mathbb{R}$$

*should impose differentiability on g*

The knowledge of the level set function is actually of limited practical utility, since nothing relevant is said about the flame front points $\mathbf{x}_f$ which is the information we desire to obtain.

**Definition 2.1.2** (**Kinematic Relations).** *It is known that the gradient of a differentiable level set function is orthogonal to that level set, therefore the normal vector* $\mathbf{n}$ *can be directly calculated from the gradient of* $G$ *and normalized. The direction points outward, i.e. from the unburnt toward the burnt since it is also*

*the direction of growing $G_0$, see figure 2.1.*

$$\mathbf{n} \equiv \frac{\nabla \mathbf{G}}{|\nabla G|} \tag{2.2}$$

*Noting that flame front velocity $\mathbf{u}_f$, is the vectorial sum of the fluid/flow velocity at the flame front $\mathbf{u}|_{G=G_0}$ and of the laminar burning velocity $-S_L\mathbf{n}$. This last term being the planar velocity at which the combustion wave would propagate from the burnt gases toward the unburnt mixture (thus the negative sign relative to the normal vector), even if the fluid where at rest, see figure 2.1.*

$$\mathbf{u}_f \equiv \mathbf{u}|_{G=G_0} - S_L\mathbf{n} \tag{2.3}$$

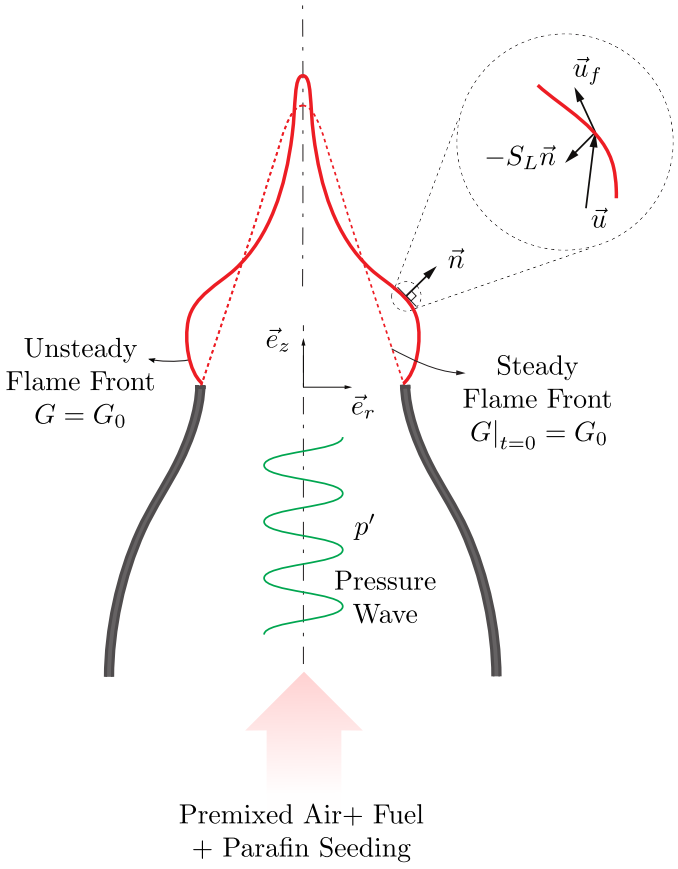


Figure 2.1: Diagram of a cross cut of a premixed burner/injector, acoustically excited, with a single, anchored unsteady flame front (red). The steady flame front (dashed red) is also represented as well a zoom on the flame region, for the analysis of the kinematic relations.

**Theorem 2.1.1** (**General G-Equation**). *Taking the total time derivative of equation (2.1), and noting that $G_0$ is a real constant.*

$$\begin{aligned} \frac{dG(\mathbf{x}_f, t)}{dt} &= \frac{\partial G}{\partial t} + \frac{d\mathbf{x}_f}{dt}\frac{\partial G}{\partial \mathbf{x}_f} = 0 \\ \frac{\partial G}{\partial t} &+ \mathbf{u}_f \cdot \nabla G = 0 \end{aligned} \tag{2.4}$$

*Substituting the flame velocity,* (2.3) *and flame normal* (2.2) *into* (2.4)*.*

$$\frac{\partial G}{\partial t} + \mathbf{u}|_{G=G_0} \cdot \nabla G - S_L \frac{\nabla \mathbf{G} \cdot \nabla G}{|\nabla G|} = 0$$
$$\frac{\partial G}{\partial t} + \mathbf{u}|_{G=G_0} \cdot \nabla G - S_L \frac{|\nabla G|^2}{|\nabla G|} = 0$$

$$\frac{\partial G}{\partial t} + \mathbf{u}|_{G=G_0} \cdot \nabla G - S_L |\nabla G| = 0 \tag{2.5}$$

missing boundary conditions (isn't this a cauchy problem???)

The determination of the points of the flame front are determined from G-equation (2.5) and with the help of definition (2.1), however the velocity field at the flame front must be prescribed ($\mathbf{u}|_{G=G_0}$), along side with a value or model for the laminar burning velocity $S_L$. Non dimensional G-Equation leads to the same equation therefore no physical significance can be attributed to it. Which makes sense it was generated out of an equilibrium of speeds

### 2.1.2 Simplified G-Equations

As mentioned on the previous section, in order to solve the G-equation, either numerically or analytically, a model for the underlying velocity field and model for the laminar burning velocity must be supplied. However there are some simplifying assumptions that can be made to the general G-equation before choosing those models. The chain of assumptions that we are about to make is sequential in most cases, thus generating G-equations of gradually more limiting domains, as seen in figure 2.2. Some assumptions have been found to be true experimentally in wide domain of flow circumstances (like axisymmetry), while other have a quite more limited range of applicability (like non-folded or tall flames).

**Assumption 2.1.1** (**Axisymmetry).** *Given that a great part of burner and injectors are circular it is usual to represent all the G-equation's functions ($G$,$\mathbf{u}$ and $S_L$) in cylindrical coordinates. Furthermore since the flows are "quite regular" it is assumed that those functions are independent from the angular coordinate $\theta$, and in the case of the flow velocity $u_\theta = 0$, i.e. axisymmetric.*

$$G(\mathbf{x}, t) = G(r, \theta, z, t) \implies G(r, z, t) \tag{2.6}$$

$$\mathbf{u}(\mathbf{x}, t) = \mathbf{u}(r, \theta, z, t) = \begin{bmatrix} u_r(r, \theta, z, t) \\ u_\theta(r, \theta, z, t) \\ u_z(r, \theta, z, t) \end{bmatrix} \implies \mathbf{u}(r, z, t) = \begin{bmatrix} u_r(r, z, t) \\ u_z(r, z, t) \end{bmatrix} \tag{2.7}$$

$$S_L(\mathbf{x}, t) = S_L(r, \theta, z, t) \implies S_L(r, z, t) \tag{2.8}$$

**Theorem 2.1.2** (**Axisymmetric G-equation).** *Introducing assumption 2.1.1 into the general G-equation*

(2.5).

$$\frac{\partial G}{\partial t} + \begin{bmatrix} u_r & u_z \end{bmatrix}\Big|_{G=G_0} \cdot \begin{bmatrix} \frac{\partial G}{\partial r} \\ \frac{\partial G}{\partial z} \end{bmatrix} - S_L \left| \begin{bmatrix} \frac{\partial G}{\partial r} \\ \frac{\partial G}{\partial z} \end{bmatrix} \right| = 0$$

$$\frac{\partial G}{\partial t} + u_r|_{G=G_0} \frac{\partial G}{\partial r} + u_z|_{G=G_0} \frac{\partial G}{\partial z} - S_L \sqrt{\left(\frac{\partial G}{\partial r}\right)^2 + \left(\frac{\partial G}{\partial z}\right)^2} = 0 \tag{2.9}$$

**Assumption 2.1.2** (**Non-Folded Flames).** *If we continue from assumption 2.1.1, and assume that the G-function is separable in the $z$ direction. The g-function is now only function of the radial direction $r$, and time $t$.*

$$G(r, z, t) = z - g(r, t) \tag{2.10}$$

*This means that the original implicit G-function is now transformed in explicit g-function $g$, which is explicit in the $z$ direction, this can be easily shown by (2.1), and (2.10).*

$$\begin{aligned} z =& g(r,t) + G_0 \quad \textit{on the flame front} \\ z =& g(r,t) \quad \textit{on the flame front with} \quad G_0 = 0 \end{aligned} \tag{2.11}$$

*An relevant observation, that gives name to this assumptions, is if the g-function is to be a function, (the arguments of $g$ have one and only one value), it cannot be folded in the $z$ direction. This assumptions has a limited range of applicability since for strongly deformed flames it has been observed in experimental setups.*

**Theorem 2.1.3** (**Non Folded g-equation).** *Introducing equation (2.10), from assumption 2.1.2, into equation (2.9), and carrying out the calculations.*

$$\frac{\partial z - g}{\partial t} + u_r|_{G=G_0} \frac{\partial z - g}{\partial r} + u_z|_{G=G_0} \frac{\partial z - g}{\partial z} - S_L \sqrt{\left(\frac{\partial z - g}{\partial r}\right)^2 + \left(\frac{\partial z - g}{\partial z}\right)^2} = 0$$

$$-\frac{\partial g}{\partial t} - u_r|_{G=G_0} \frac{\partial g}{\partial r} + u_z|_{G=G_0} - S_L \sqrt{\left(\frac{\partial g}{\partial r}\right)^2 + 1} = 0 \tag{2.12}$$

**Assumption 2.1.3** (**Tall, Monotonic Flames).** *This assumption arises from the need to simplify the modulus and the square root it originates, in the g-equation (2.12).*

$$\left(\frac{\partial g}{\partial r}\right)^2 \gg 1 \quad \textit{and} \quad \frac{\partial g}{\partial r} \leq 0 \tag{2.13}$$

**Theorem 2.1.4** (**Tall g-equation).** *Imposing the tall flame assumption (2.1.3) into the non-folded g-equation* (2.12).

$$-\frac{\partial g}{\partial t} - u_r|_{G=G_0}\frac{\partial g}{\partial r} + u_z|_{G=G_0} - S_L\left|\frac{\partial g}{\partial r}\right| = 0 \tag{2.14}$$

**Assumption 2.1.4** (**Separable, Time Harmonic g-function).** *This assumption arises as way to transform the partial differential g-equation into a ordinary differential equation.Why are we assuming this? Mathematical reaseoning seems weak.*

$$g(r,t) = \bar{g}(r) + g'(r)e^{-i\omega t} \tag{2.15}$$

**Theorem 2.1.5** (**Non-Folded Ordinary g-equation).** *Introducing assumption 2.1.4, into equation* (2.12).

$$i\omega g' e^{-i\omega t} - u_r|_{G=G_0}\left(\frac{\partial \bar{g}}{\partial r} + \frac{\partial g'}{\partial r}e^{-i\omega t}\right) + u_z|_{G=G_0} - S_L\sqrt{\left(\frac{\partial \bar{g}}{\partial r} + \frac{\partial g'}{\partial r}e^{-i\omega t}\right)^2 + 1} = 0 \tag{2.16}$$

*This equation is still strongly coupled between steady and oscillating terms, especially due the terms inside the square root.*

**Theorem 2.1.6** (**Tall Ordinary g-equation).**

$$i\omega g' e^{-i\omega t} - u_r|_{G=G_0}\left(\frac{\partial \bar{g}}{\partial r} + \frac{\partial g'}{\partial r}e^{-i\omega t}\right) + u_z|_{G=G_0} - S_L\left|\frac{\partial \bar{g}}{\partial r} + \frac{\partial g'}{\partial r}e^{-i\omega t}\right| = 0 \tag{2.17}$$

As summary of this section, we represent all the equations deduced, according to the consecutive assumptions in flowchart 2.2. We start with the general G-equation (2.5), the axisymmetric assumptions 2.1.1 then generates the axisymmetric G-equation (2.9), then we add the non-folded assumption 2.1.2 and this produces the non-folded g-equation (2.12). From the non-folded g-equation we apply the tall flame assumption 2.1.3 producing the tall g-equation (2.14). Finally we apply the g-function separable time harmonic assumption 2.1.4, however this assumption can be applied to both the non-folded g-equation (2.12), and the tall g-equation (2.14), producing respectively the non-folded ordinary (2.16), and tall ordinary (2.17).

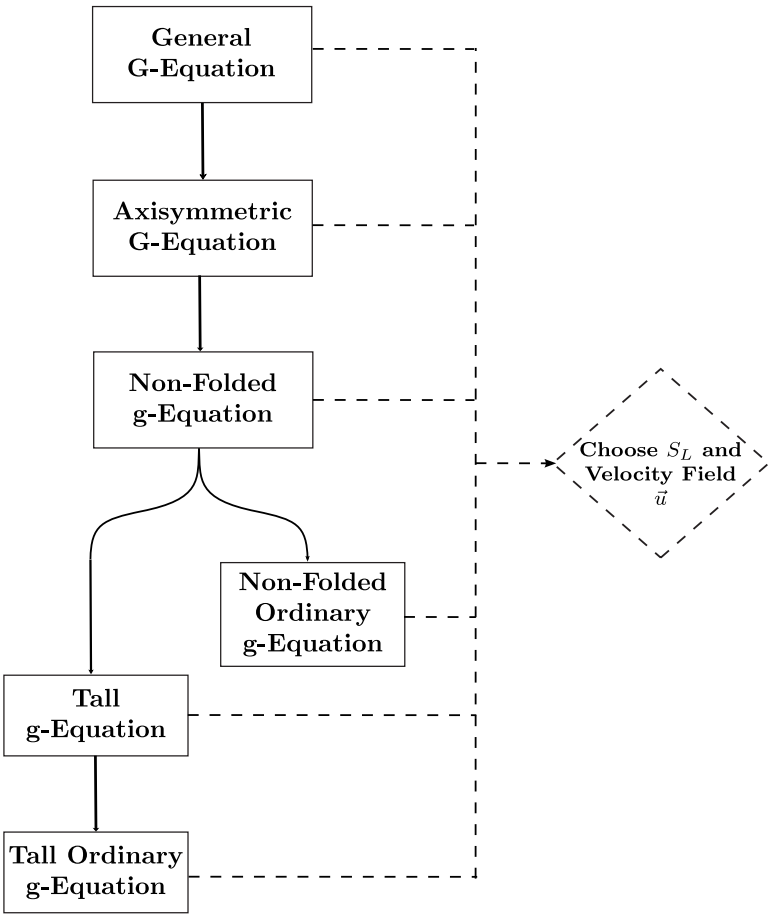


Figure 2.2: Flow chart that represents the cascading of simplified G-equations from the most general on top to least on the bottom. It can be used to choose a desired level of approximation, then after reaching the desired level we must always follow up to a modeling of flow velocity and laminar burning velocity.

### 2.1.3 G-operators

$$\mathcal{G}_{gen}(G,\mathbf{u},S_L) = \frac{\partial G}{\partial t} + \frac{\partial G}{\partial x_j}\, u_j|_{G=G_0} - S_L\sqrt{\frac{\partial G}{\partial x_j}\frac{\partial G}{\partial x_j}} \tag{2.18}$$

$$\mathcal{G}_{axi}(G,\mathbf{u},S_L) = \frac{\partial G}{\partial t} + \frac{\partial G}{\partial r}\, u_r|_{G=G_0} + \frac{\partial G}{\partial z}\, u_z|_{G=G_0} - S_L\sqrt{\left(\frac{\partial G}{\partial r}\right)^2 + \left(\frac{\partial G}{\partial z}\right)^2} \tag{2.19}$$

$$\mathcal{G}_{nfold}(g,\mathbf{u},S_L) = -\frac{\partial g}{\partial t} - \frac{\partial g}{\partial r}\, u_r|_{G=G_0} + u_z|_{G=G_0} - S_L\sqrt{\left(\frac{\partial g}{\partial r}\right)^2 + 1} \tag{2.20}$$

$$\mathcal{G}_{tall}(g,\mathbf{u},S_L) = -\frac{\partial g}{\partial t} - \frac{\partial g}{\partial r}\, u_r|_{G=G_0} + u_z|_{G=G_0} - S_L\frac{\partial g}{\partial r} \tag{2.21}$$

Testing linearity and bilinearity of Tall G-operator

$$\mathcal{G}_{Tall}(g=\bar{g}(r)+\tilde{g}(r),\mathbf{u},S_L) = \mathcal{G}_{Tall}(g=\bar{g}(r),\mathbf{u},S_L) + \mathcal{G}_{Tall}(g=\tilde{g}(r,t),\mathbf{u},S_L)$$

$$\mathcal{G}_{tall}(g=\bar{g}(r)+\tilde{g}(r,t),\mathbf{u},S_L) = -\frac{\partial \tilde{g}}{\partial t} - \left(\frac{\partial \bar{g}}{\partial r} + \frac{\partial \tilde{g}}{\partial r}\right) u_r|_{G=G_0} + u_z|_{G=G_0} + S_L\left(\frac{\partial \bar{g}}{\partial r} + \frac{\partial \tilde{g}}{\partial r}\right)$$

$$\mathcal{G}_{tall}(g=\bar{g}(r),\mathbf{u},S_L) = -\frac{\partial \bar{g}}{\partial r}\, u_r|_{G=G_0} + u_z|_{G=G_0} + S_L\frac{\partial \bar{g}}{\partial r}$$

$$\mathcal{G}_{tall}(g=\tilde{g}(r),\mathbf{u},S_L) = -\frac{\partial \tilde{g}}{\partial t} - \frac{\partial \tilde{g}}{\partial r}\, u_r|_{G=G_0} + u_z|_{G=G_0} + S_L\frac{\partial \tilde{g}}{\partial r}$$

## 2.2 Flame Transfer Functions

In order to encapsulate the knowledge of the thermoacoustic response of a system, from a control theory perspectiveseveral approaches are possible, but one of the most used is the transfer function. The flame transfer function *FTF* is therefore a simplification of flame system, but containing it's essential dynamic behavior to external disturbances. Since the Rayleigh Criterion postulates that the coupling of heat release and pressure oscillations could lead to instability, the heat release response to pressure oscillations would be good a transfer functions. However pressure is usually only possible to measure by intrusive techniques it usual preferred to user velocity oscillations since they also capture the acoustic field information but can be measured unobtrusively by laser Doppler velocimetry (*LDV*). The FTF is usually presented in a non dimensional form therefore it custom to make it dimensionless by dividing both the velocity oscillations and heat release oscillations by their average values, therefore:

$$FTF \equiv \frac{\dfrac{Q'}{\bar{Q}}}{\dfrac{u'_z}{\bar{u}_z}}$$

But the heat release could be calculated from (explain better)

$$Q = \int \rho_{mix} S_L q_{reac} dA_f$$

If the mixture density $\rho_{mix}$, reaction heat per unit of mass $q_{reac}$, and laminar burning velocity $S_L$ are all constant the heat release would be proportional to the flame area $A_f$ only, therefore. Also important to note is that the velocity ratios $\frac{u'_z}{\bar{u}_z}$ might depend on $r$ and therefore FTF also depends on which is a quite undesired consequence, since the FTF should model the entire flame and so depend only on the input amplitude and frequency. To remediate this property it is usual to take the velocity ratio on the middle line i.e. $r = 0$.

$$FTF \equiv \frac{\frac{Q'}{\bar{Q}}}{\frac{u'_z}{\bar{u}_z}} = \frac{\frac{A'}{\bar{A}}}{\left.\frac{u'_z}{\bar{u}_z}\right|_{r=0}}$$

Introducing 2.26 and 2.25

$$FTF = \frac{\frac{\int_0^R r \left|\frac{\partial g'}{\partial r}\right| dr}{\int_0^R r \left|\frac{\partial \bar{g}}{\partial r}\right| dr}}{\left.\frac{u'_z}{\bar{u}_z}\right|_{r=0}}$$

Another possible definition for the flame transfer function, which removes the explicit dependency of the $r$, could be done by taking the volumetric flow rate, i.e. taking the integral of the velocity quantities. The volumetric flow rate in cylindrical coordinates is given by:

$$\begin{aligned}
\dot{V}_z &\equiv \int_0^{2\pi} \int_0^R u_z r dr d\theta \\
\dot{V}_z &= 2\pi \int_0^R \bar{u}_z r dr + 2\pi \int_0^R u'_z e^{-i\omega(t-\tau)} r dr \\
\dot{V}_z &= \bar{\dot{V}} + \dot{V}' e^{-i\omega(t-\tau)} \\
\bar{\dot{V}}_z &= 2\pi \int_0^R \bar{u}_z r dr \\
\dot{V}'_z &= 2\pi \int_0^R u'_z r dr
\end{aligned}$$

And hence a new type of FTF is proposed based in the volumetric flow rate.

$$FTF_{\dot{V}} \equiv \frac{\frac{A'}{\bar{A}}}{\frac{\dot{V}'_z}{\bar{\dot{V}}_z}} = \frac{\frac{\int_0^R r \left|\frac{\partial g'}{\partial r}\right| dr}{\int_0^R r \left|\frac{\partial \bar{g}}{\partial r}\right| dr}}{\frac{\int_0^R u'_z r dr}{\int_0^R \bar{u}_z r dr}}$$

Since we considered the flame as axisymmetric (around the $z$ axis) its instantaneous surface area $A_f(t)$, is given has a integral of revolution of $g(r,t)$

$$A_f(t) = 2\pi \int_0^R r\sqrt{\left(\frac{\partial g}{\partial r}\right)^2 + 1}dr \tag{2.22}$$

$$A_f(t) = 2\pi \int_0^R r\left|\frac{\partial g}{\partial r}\right| dr$$

$$A_f(t) = 2\pi \int_0^R \left(\left|r\frac{\partial \bar{g}}{\partial r}\right| + r\left|\frac{\partial g'}{\partial r}\right| e^{-i\omega t}\right) dr \tag{2.23}$$

$$A_f(t) = \bar{A}_f + A'_f e^{-i\omega t} \tag{2.24}$$

$$\bar{A}_f = 2\pi \int_0^R r\left|\frac{\partial \bar{g}}{\partial r}\right| dr \tag{2.25}$$

$$A'_f = 2\pi \int_0^R r\left|\frac{\partial g'}{\partial r}\right| dr \tag{2.26}$$

## 2.3 Modeling Flow Velocity Field

We can either supply a analytical velocity field or use experimental or computational approaches to obtain the velocity field. We choose the second approach and provide a analytical flow field that has quite general mathematical form, and also quite "strong" experimental evidence.

**Assumption 2.3.1** (**Uniaxial, Separable, Traveling Wave Flow Velocity).** *There have been experimental evidence that radial velocity component is negligible, since by velocimetry techniques (LDV or PIV for example) the flow speed can be determined with quite high precision.*

$$u_r = 0 \tag{2.27}$$

*For the axial velocity component $u_z$ is possible to express the underlying flow assuming it as a uniform base flow $\bar{u}_z$, and adding a traveling wave in the $z$ direction, with wave number $k$ and angular frequency $\omega$, these kind of general wave like behavior is see in several other physical problems like acoustics, electromagnetism and quantum mechanics.*

$$u_z(r,z,t) = \bar{u}_z(r) + u'_z(r)e^{i(kz-\omega t)}$$

*The wave number $k$, can be related with a propagation wave phase velocity $v_p$, as well as the relation between angular frequency $\omega$ and wave frequency $f$.*

$$\omega = 2\pi f \tag{2.28}$$

$$k = \frac{\omega}{v_p} = \frac{2\pi f}{v_p} \tag{2.29}$$

*Thus axial velocity is given by:*

$$u_z(r,z,t) = \bar{u}_z(r) + u'_z(r)e^{i\omega\left(\frac{z}{v_p} - t\right)} \tag{2.30}$$

The angular frequency $\omega$ is usually a input for the system, as we will see further on the flame transfer functions, from experimental point of view it is this frequency that is set on the loudspeaker the excites the system, in order to generate the velocity oscillation. However the wave phase velocity $v_p$ is a little more debatable since from a physical point of view, what would make sense is that should be about the same has the flow average velocity $\bar{u}_z$, however from a acoustic point of view it is interesting to note that a wave is also generated on top of this flow, and it propagates with the speed of sound $c$, however with a much smaller amplitude.

some suggest that $v_p \neq \bar{u}_z$ **?**, **?**

**Assumption 2.3.2** (**Flow Average Wave Propagation).**

$$v_p = \bar{u}_z \tag{2.31}$$

$$u_z = \bar{u}_z(r) + u'_z(r)e^{i\omega\left(\frac{z}{\bar{u}_z} - t\right)} \tag{2.32}$$

**Assumption 2.3.3** (**Infinite Wave Propagation).** *In the limit of $u_z$ when the $v_p$, tend toward infinity the velocity field becomes.*

$$\lim_{v_p \to \infty} u_z = \lim_{v_p \to \infty} \bar{u}_z(r) + u'_z(r)e^{i\omega\left(\frac{z}{v_p} - t\right)}$$

$$\lim_{v_p \to \infty} u_z = \bar{u}_z + u'_z e^{-i\omega t} \tag{2.33}$$

*Assuming that the flow velocity wave propagates in the $z$, direction with infinite velocity is an unrealistic assumption however it is still of important to understand these limiting cases, and also help decouple the ordinary differential equations as we see later on.*

## 2.4 Modeling Laminar Burning Velocity

The laminar burning velocity $S_L$, has dependencies of several parameters, like the chemical composition of the fuel, temperature, pressure, equivalence ratio, etc. However since G-equation is a kinematic model we focus only on the flame geometry dependencies, and underling flow field dependencies, the only parameters on equation (2.5).

The studies carried out by Markstein, Calvin and Williams, according to **?**, culminated in a model, that for the case, of flames with ratios of flame thickness to wavelength much smaller than unity $\frac{\delta_f}{\Lambda} \ll 1$, a written as first order model. what does this ratio mean?

**Assumption 2.4.1** (**First Order $S_L$ Model).**

$$S_L = S_L^0 + \mathscr{L}\left(\frac{1}{\delta A}\frac{d\delta A}{dt}\right) + \mathcal{O}(...)$$

$$S_L = S_L^0 + \mathscr{L}\alpha \tag{2.34}$$

$$\alpha \equiv \frac{1}{\delta A}\frac{d\delta A}{dt} \tag{2.35}$$

*The model proposed in (2.34), has the $S_L^0$, which is the adiabatic laminar burning velocity under non-stretched conditions, and $\mathscr{L}$ is the Markstein length which represents the sensitivity of the flame response to stretch effects. Also due to Calvin is the conceptual/phenomenological separation of the stretch parameter $\alpha$, in several separate effects, such as for example strain rate $\alpha_s$, flame curvature $\alpha_c$, and even pressure or other experimentally observable parameters.*

$$S_L = S_L^0 + \mathscr{L}_s\alpha_s + \mathscr{L}_c\alpha_c + \mathscr{L}_p\alpha_p + ...$$

$$S_L = S_L^0 + \mathscr{L}_s\alpha_s + \mathscr{L}_c\alpha_c \tag{2.36}$$

*Where the new Markstein lengths are introduced for each of the components, in this study we focus on the kinematics, so the relevant are the Markstein strain length $\mathscr{L}_s$, and the Markstein curvature length $\mathscr{L}_c$, therefore our models is simply.*

**Theorem 2.4.1** (**Candel-Poinsot Stretch Equivalence).** *In **?**, Candel and Poinsot not only obtained a model for the strain and curvature components, but created a more general formulation for the transport of the flame flux quantities like the flame normal $\mathbf{n}$ and the flame curvature $\nabla \cdot \mathbf{n}$.*

$$\alpha = \alpha_s + \alpha_c \tag{2.37}$$

$$\alpha_s = -\mathbf{nn} : \nabla\mathbf{u} + \nabla \cdot \mathbf{u} \tag{2.38}$$

$$\alpha_c = S_L \nabla \cdot \mathbf{n} \tag{2.39}$$

*sl has been defined implicitly. something is wrong here*

**Assumption 2.4.2** (**Constant Laminar Burning Velocity).** *To simplify the modeling it is usual to as-*

*sume that the laminar burning velocity is constant.*

$$S_L = S_L^0 \tag{2.40}$$

**Assumption 2.4.3** (**Area Average $S_L$ Model).**

$$\alpha_{\bar{A}_f} \equiv \frac{\int_{\bar{A}_f} \alpha \delta A}{\int_{\bar{A}_f} \delta A} = \frac{\int_{\bar{A}_f} \frac{1}{\delta A} \frac{d\delta A}{dt} \delta A}{\int_{\bar{A}_f} dA} = \frac{\frac{d}{dt}\left(\int_{\bar{A}_f} \delta A\right)}{\int_{\bar{A}_f} \delta A} = \frac{1}{\bar{A}_f} \frac{d\bar{A}_f}{dt}$$

## 2.5 G-Models

From the flowchart 2.2, we can see that there are several G/g-equations and with several velocity and laminar burning velocity models it is possible to generate quite a big number of different G/g models. However on the this study we will focus on models that have a constant burning velocity 2.4.2, and a traveling wave velocity field 2.3.1, and all the g-equations that are axisymmetric or further simplified, since our imposed velocity field already is axisymmetric.

**Theorem 2.5.1** (**Axisymmetric G-equation with Constant $S_L$ and Uniaxial Traveling Wave Velocity Field).** *Taking the axisymmetric G-equation* (2.9)*, and applying the constant $S_L$ assumption 2.4.2 and a velocity field of assumption 2.3.2.*

$$\frac{\partial G}{\partial t}+\frac{\partial G}{\partial z}\left(\bar{u}_z(r)+u'_z(r)e^{i\omega\left(\frac{z}{\bar{u}_z}-t\right)}\right)\Bigg|_{G=G_0}-S_L^0\sqrt{\left(\frac{\partial G}{\partial r}\right)^2+\left(\frac{\partial G}{\partial z}\right)^2}=0 \tag{2.41}$$

*Solutions for this equation can only be expect by implementation of numerical methods. It is a 1D time + 2D space, non-linear, first order partial differential equation.*

**Theorem 2.5.2** (**Non-Folded g-equation with Constant $S_L$ and Uniaxial Traveling Wave Velocity Field).** *Using the non-folded g-equation* (2.12)*, with the velocity field of assumption 2.3.2, and constant burning velocity.*

$$-\frac{\partial g}{\partial t}+\left(\bar{u}_z(r)+u'_z(r)e^{i\omega\left(\frac{z}{\bar{u}_z}-t\right)}\right)\Bigg|_{G=G_0}-S_L^0\sqrt{\left(\frac{\partial g}{\partial r}\right)^2+1}=0$$

*From equation* (2.11) *non-folded assumption 2.1.2 allows us replace $z$.*

$$-\frac{\partial g}{\partial t}+\bar{u}_z(r)+u'_z(r)e^{i\omega\left(\frac{g}{\bar{u}_z}-t\right)}-S_L^0\sqrt{\left(\frac{\partial g}{\partial r}\right)^2+1}=0 \tag{2.42}$$

*This equation is a 1D time + 1D space non-linear first order differential equation. Thus the non folded assumption reduced one spatial dimension, which might quite significant from numerical point of view.*

**Theorem 2.5.3** (**Tall g-equation with Constant $S_L$ and Uniaxial Traveling Wave Velocity Field).** *Proceeding in similar way but now with the tall g-equation*

$$-\frac{\partial g}{\partial t}+\bar{u}_z(r)+u'_z(r)e^{i\omega\left(\frac{g}{\bar{u}_z}-t\right)}-S_L^0\left|\frac{\partial g}{\partial r}\right|=0 \tag{2.43}$$

**Theorem 2.5.4** (**Non-folded Ordinary g-equation with Constant $S_L$ and Uniaxial Traveling Wave Velocity Field).**

$$i\omega g' e^{-i\omega t}+\bar{u}_z(r)+u'_z(r)e^{i\omega\left(\frac{\bar{g}+g'e^{-i\omega t}}{\bar{u}_z}-t\right)}-S_L^0\sqrt{\left(\frac{\partial \bar{g}}{\partial r}+\frac{\partial g'}{\partial r}e^{-i\omega t}\right)^2+1}=0 \tag{2.44}$$

**Theorem 2.5.5** (**Non-folded Tall Ordinary g-equation with Constant $S_L$ and Uniaxial Traveling Wave Velocity Field).**

$$i\omega g' e^{-i\omega t} + \bar{u}_z(r) + u_z'(r) e^{i\omega\left(\frac{\bar{g}+g'e^{-i\omega t}}{\bar{u}_z} - t\right)} - S_L^0 \left| \frac{\partial \bar{g}}{\partial r} + \frac{\partial g'}{\partial r} e^{-i\omega t} \right| = 0 \tag{2.45}$$

*but this equation is not separable in steady and oscillating as ivo suggested (and uses)*

$$\bar{u}_z(r) - S_L^0 \left| \frac{\partial \bar{g}}{\partial r} \right| = 0 \tag{2.46}$$

$$i\omega g' e^{-i\omega t} + u_z'(r) e^{i\omega\left(\frac{\bar{g}+g'e^{-i\omega t}}{\bar{u}_z} - t\right)} - S_L^0 \left| \frac{\partial g'}{\partial r} e^{-i\omega t} \right| = 0 \tag{2.47}$$

| G-equation Type | $v_p = \bar{u}_z$ and $S_L^0$ | $v_p = \infty$ and $S_L^0$ |
|---|---|---|
| Axisymetric Non-Folded Tall Ordinary Non-Folded Ordinary Tall | | |

Table 2.1:

# Chapter 3

# Experimental Methods

In the overall work of this thesis a great amount of effort was put into experimental methods since they provide the only true mechanism to validate most of the the assumptions proposed in the previous chapters. The experimental approach of this thesis can be divided into two major areas, first the need to measure flow fields inside the flame since they provide validation to the velocity model proposed in 2.3. The precise measurement of flow fields, that will server as initial condition for the numerical model, are obtained via Laser Doppler Velocimetry (*LDV*) which is described in 3.2.1. The second area of experimental methodology is the tracking of flame front positions via a high speed camera system. These visualization methods provides direct validation for the results obtained when solving the G-Equation's, since there solution provides flame front positions, and velocities. However before we proceed to an in depth description of the these experimental methods we provide an overall description of the experimental setup.

## 3.1 Experimental Setup

The experimental setup consists of cylindrical, propane premixed plenum burner shown in figure 3.1. The plenum chamber is supplied with propanene and air from digitally mass flow controller, figure 3.2. These flow controllers get supplied from the laboratory propane and air main conducts. The digital flow controllers allow the plenum chamber to be supplied with a steady laminar flow in STP conditions and mimizes in realtime to pressure fluctuations in the main conducts.

## 3.2 Experimental Techniques

### 3.2.1 Laser Doppler Velocimetry

### 3.2.2 High Speed Flame Imagery

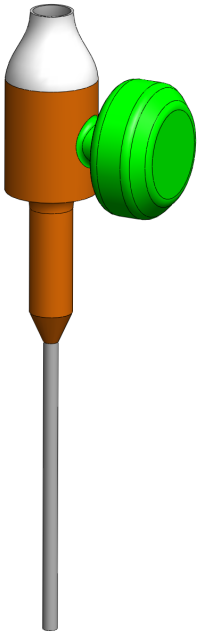

(a) CAD representation of the burner used. In green the loudspeaker is represented.

Figure 3.1: Foto and schematic of the burner used.


(a) CAD representation of the burner used. In green the loudspeaker is represented.

Figure 3.2: Foto and schematic of the burner used.

# Chapter 4

# Conclusions